Häusler, K., Lühr, H., Hagan, M. E., Maute, A., Roble, G.R. (2010): Comparison of CHAMP and TIME-GCM nonmigrating tidal signals in the thermospheric zonal wind. - Journal of Geophysical Research, 115, D00I08

DOI: 10.1029/2009JD012394

JOURNAL OF GEOPHYSICAL RESEARCH, VOL. 115, D00I08, doi:10.1029/2009JD012394, 2010

Comparison of CHAMP and TIME-GCM nonmigrating tidal signals in the thermospheric zonal wind

K. Häusler,[1] H. Lühr,[1] M. E. Hagan,[2] A. Maute,[2] and R. G. Roble[2]

Received 30 April 2009; revised 28 August 2009; accepted 6 October 2009; published 27 February 2010.

[1] Four years (2002–2005) of continuous accelerometer measurements taken onboard the CHAMP satellite (orbit altitude ~400 km) offer a unique opportunity to investigate the thermospheric zonal wind on a global scale. Recently, we were able to relate the longitudinal wave-4 structure in the zonal wind at equatorial latitudes to the influence of nonmigrating tides and in particular to the eastward propagating diurnal tide with zonal wave number 3 (DE3). The DE3 tide is primarily excited by latent heat release in the tropical troposphere in deep convective clouds. In order to investigate the mechanisms that couple the tidal signals to the upper thermosphere, we undertook a comparison with the thermosphere-ionosphere-mesosphere-electrodynamics general circulation model (TIME-GCM) developed at the National Center for Atmospheric Research (NCAR). We ran the model for a day in March, June, September, and December and applied the same processing steps to the model output as was done for the CHAMP tidal analysis. The main results of the comparison can be summarized as follows: (1) TIME-GCM simulations do not correctly reproduce the observed intra-annual variations of DE3 and the eastward propagating diurnal tide with zonal wave number 2 (DE2). (2) Simulations of DE3 for June are more successful. Both TIME-GCM and CHAMP show an increase in DE3 amplitudes with decreasing solar flux level. (3) The amplitudes of the simulated westward propagating diurnal tide with zonal wave number 2 (DW2) and the standing diurnal tide (D0) increase with increasing solar flux in June. The predicted dependence of DW2 and DO on solar flux is also observed by CHAMP.

Citation: Häusler, K., H. Lühr, M. E. Hagan, A. Maute, and R. G. Roble (2010), Comparison of CHAMP and TIME-GCM nonmigrating tidal signals in the thermospheric zonal wind, *J. Geophys. Res.*, *115*, D00I08, doi:10.1029/2009JD012394.

1. Introduction

[2] Numerous satellite missions, e.g., TIMED (Thermosphere Ionosphere Mesosphere Energetics and Dynamics), ROCSAT-1 (Republic of China Satellite 1), and CHAMP (Challenging Minisatellite Payload), provide innovative continuous and globally distributed measurements of the parameters of the upper atmosphere. Thereby, growing evidence is presented that upward propagating tides from as low as the troposphere are able to modulate upper atmospheric quantities. According to tidal theory some of those tides are referred to as nonmigrating tides and, unlike migrating tides, they are non-Sun-synchronous [e.g., *Chapman and Lindzen*, 1970; *Forbes*, 1995]. That is, they can propagate eastward (E), westward (W) or remain standing with any given zonal wave number *s*. Diurnal (D) oscillations have a period of 24 h, while semidiurnal (S) oscillations have a period of 12 h. Throughout this paper we will use the letter/number combination *DWs* (*SWs*) and *DEs* (*SEs*) to describe a westward or eastward propagating diurnal (semidiurnal) tide with zonal wave number *s*. Standing tidal oscillations are termed *D0* and *S0*, while stationary planetary waves with zonal wave number *m* are labeled as *sPWm*.

[3] An important nonmigrating tide is DE3. The origin of DE3 is the tropical troposphere where it is excited by latent heat release in deep convective clouds [*Hagan and Forbes*, 2002]. The presence of DE3 in the mesosphere and lower thermosphere region (MLT) has been reported by *Forbes et al.* [2006, 2008] and *Zhang et al.* [2006] in temperature and by *Oberheide et al.* [2006] and *Wu et al.* [2008] in zonal and meridional wind. But the ionosphere is also influenced by DE3. *Sagawa et al.* [2005] were the first to report a four-peaked ("wave-4") longitudinal structure of the *F* region equatorial ionization anomaly (EIA) and *Immel et al.* [2006] attributed the longitudinal variation to the presence of DE3 which is evident as a wave-4 structure when observed from Sun-synchronous orbits. Soon after, reports of DE3 signatures in the electron density [e.g., *Lin et al.*, 2007; *Lühr et al.*, 2007], electric field [e.g., *Hartman and Heelis*, 2007; *Kil et al.*, 2007], and electrojet [e.g., *England et al.*, 2006; *Lühr et al.*, 2008] followed.

[4] *Häusler et al.* [2007] report on a dominant wave-4 structure seen in the CHAMP zonal wind at 400 km altitude during certain local times (LT). In a recent study, *Häusler and Lühr* [2009] were able to relate the identified wave-4

[1]Helmholtz Centre Potsdam–GFZ German Research Centre for Geosciences, Potsdam, Germany.
[2]High Altitude Observatory, National Center for Atmospheric Research, Boulder, Colorado, USA.

0148-0227/10/2009JD012394$09.00

pattern in the zonal wind to the presence of DE3. Analyzing CHAMP and GRACE (Gravity Recovery And Climate Experiment) accelerometer measurements, *Forbes et al.* [2009] also found DE3 signatures in exosphere temperature. Performing numerical experiments with the thermosphere-ionosphere-mesosphere-electrodynamics general circulation model (TIME-GCM), *Hagan et al.* [2007] explored the effects of tides with tropospheric sources on the upper and middle atmosphere. Thereby the authors show that DE3 is capable of penetrating from the troposphere to the thermosphere. Furthermore, the nonlinear interaction between the DE3 and the migrating diurnal tide (DW1) generates a stationary planetary wave-4 oscillation (sPW4) in the mesosphere and lower thermosphere (MLT) region which may have an impact on the E region dynamo as well as the atmospheric dynamics further aloft [*Hagan et al.*, 2009]. Using Hough Mode Extensions (HMEs) to connect the observed TIMED tides with the CHAMP tides, *Oberheide et al.* [2009] demonstrate that the upper thermospheric DE3 tidal winds and exosphere temperatures are fully attributable to direct tidal upward propagation from the troposphere. Yet, an open issue is the stronger CHAMP DE3 tidal wind observed along the dip equator as compared with the geographic equator. Deep convective clouds are not controlled by the geomagnetic field, thus the largest DE3 amplitudes should be found along the geographic equator. Another interesting result of the *Oberheide et al.* [2009] study is the reported solar cycle dependence of the DE3 tidal zonal wind in the upper thermosphere. Larger amplitudes of DE3 are observed during solar minimum conditions. However, besides the important DE3, there are also other nonmigrating tides, e.g., DE2, present in the upper thermosphere [*Forbes et al.*, 2009; *Häusler and Lühr*, 2009].

[5] In this report, we explore in situ measurements from CHAMP and TIME-GCM simulations in order to quantify nonmigrating tidal signatures in the upper thermospheric zonal wind and assess the performance of the model, because reliable model simulations are needed to understand the governing processes behind the coupling from the troposphere to the thermosphere.

2. Model and Data Analysis

[6] TIME-GCM is a three-dimensional time-dependent global grid point model that calculates the dynamics, electrodynamics, photoionization, neutral gas heating, and the compositional structure of the middle and upper atmosphere. A more complete description of the model, which was developed at the National Center for Atmospheric Research, is given by *Roble* [1995, 1996], *Roble and Ridley* [1994] and references therein. TIME-GCM is able to inherently calculate the atmospheric tides that are excited by the absorption of ultraviolet and extreme ultraviolet radiation in the middle and upper atmosphere. Nevertheless, it cannot account for tidal components that are excited by latent heat release in deep tropical clouds or by the absorption of infrared radiation [*Hagan et al.*, 2007]. In order to introduce the tides of tropospheric origin into TIME-GCM, the lower boundary (i.e., 10 mb; ~30 km) of the model is driven by results of the global-scale wave model (GSWM) which can account for the missing tides [e.g., *Hagan and Forbes*, 2002, 2003].

[7] For the simulations discussed herein, we ran TIME-GCM with 2.5° by 2.5° horizontal resolution, 4 grid points per scale height in the vertical, and we let it settle to a diurnally reproducible state for the fifteenth day in March, June, September, and December during solar minimum conditions. Thus, the 10.7 cm solar radio flux (F10.7) value was set to 75 sfu (sfu = 10^{-22} m^{-2} Hz^{-1}), the hemispheric power value [after *Evans*, 1987] to 8 GW, and the cross-cap potential drop to 30 kV. The June simulations were also run for moderate (120 sfu) and high (200 sfu) solar flux levels.

[8] The CHAMP data set used for comparison with TIME-GCM is the same as described by *Häusler and Lühr* [2009]. In the aforementioned study, 4 years of CHAMP zonal wind measurements taken between 2002 and 2005 have been analyzed for nonmigrating tidal signatures in the upper thermosphere. CHAMP is revolving around Earth on a circular, near polar orbit at an inclination of 87.3° since its launch in July 2000. The satellite is precessing through 24 h LT within 261 days, taking about 11 days for 1 h LT precession. Combining the ascending and descending node of the satellite yields 24 h LT coverage within 131 days. The desired tidal spectrum is obtained by performing a two-dimensional Fourier analysis on the preprocessed zonal wind residuals as described by *Häusler and Lühr* [2009]. Thereby, 24 h LT coverage is a mandatory requirement and 24 h LT coverage for each month of the year is approximately achieved by merging 4 years of measurements. The main processing steps before performing the two-dimensional Fourier analysis include removing a daily zonal mean from an orbit arc averaged over a selected latitude band [*Häusler et al.*, 2007] and sorting the obtained zonal wind residuals into months, LT intervals, and longitude bins [*Häusler and Lühr*, 2009]. Notably, we cannot resolve any migrating tidal signatures, since both the zonal mean zonal winds and the longitude invariant migrating tidal zonal wind signatures are removed in the preliminary processing of the CHAMP data. The satellite altitude changes over time (~35 km within the 4 years) but because the tides have a large vertical wavelength [e.g., *Talaat and Lieberman*, 1999] this change is not detrimental to the analysis.

[9] In order to make reasonable comparisons, the TIME-GCM output was processed in the same way as the CHAMP data. The standard TIME-GCM output is in universal time (UT), requiring that we first transfer the model data into the LT system of the satellite. After that we applied the same aforementioned processing steps on the TIME-GCM zonal winds near 400km which yielded the model tidal spectra. Due to the model resolution, the latitude bin around the equator ranges from 11.25°N to 11.25°S for TIME-GCM compared to 10°N to 10°S for CHAMP.

[10] *Häusler and Lühr* [2009] report that the sorting of the zonal wind residuals into LT intervals and longitude bins induces a damping on the tidal amplitudes. The amplitudes reported herein have been corrected for this effect.

3. Results

[11] We ran our solar minimum simulations with an F10.7 value of 75 and let the model settle to a diurnally reproducible state for March, June, September, and December.

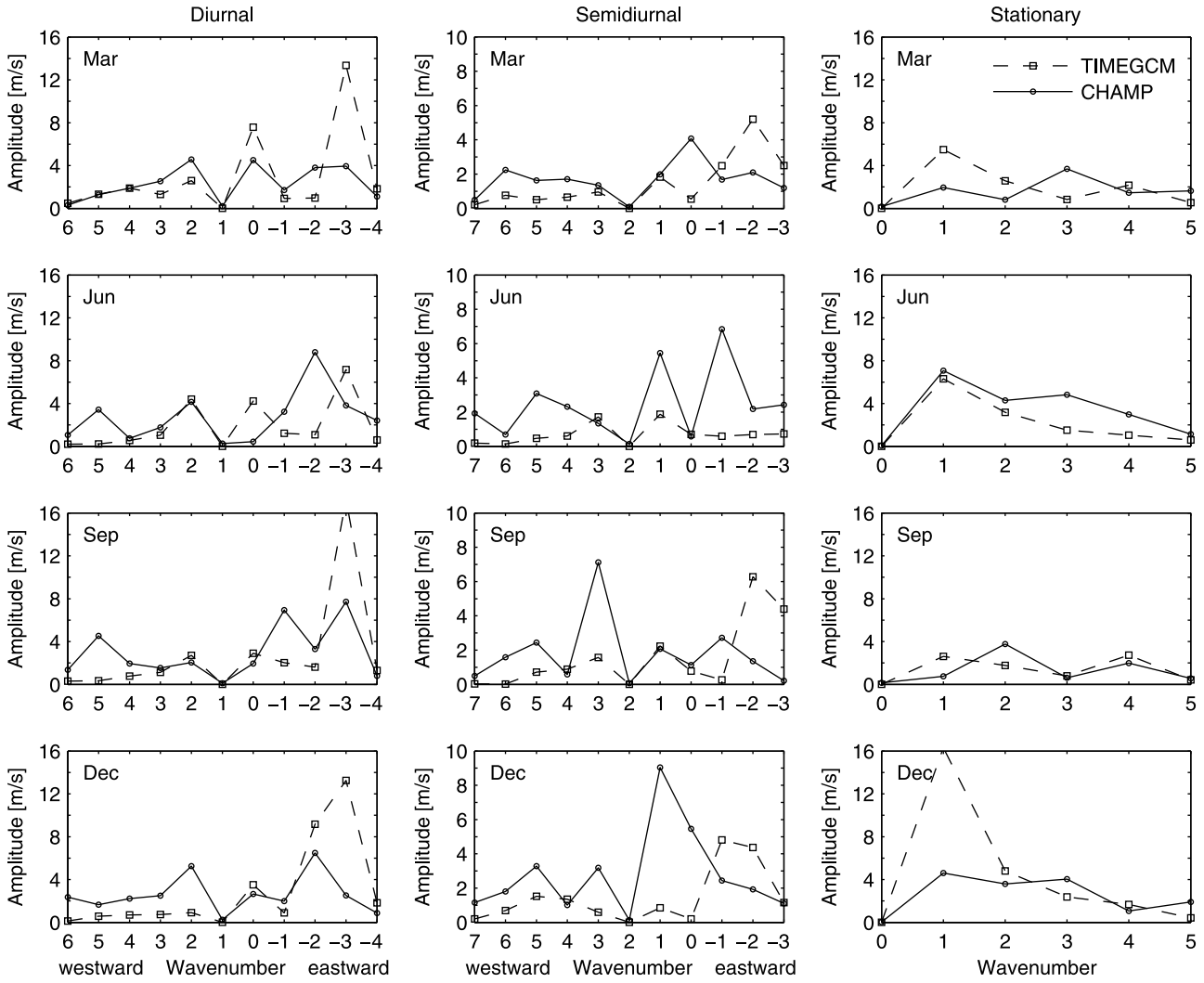

Figure 1. Tidal spectra for TIME-CM (dashed line with squares) and CHAMP (solid line with circles) of zonal winds for the months of (top to bottom) March, June, September, and December for (left) diurnal, (middle) semidiurnal, and (right) stationary components. Positive (negative) wave numbers correspond to westward (eastward) propagating tides.

The GSWM lower boundary forcing included westward propagating zonal wave number 6 (W6) through eastward propagating zonal wave number 6 (E6) diurnal and semidiurnal components. The resolvable tides from CHAMP measurements range from DW6 to DE4 for the diurnal, from SW7 to SE3 for the semidiurnal tides, and from sPW1 to sPW5 for the stationary planetary waves. They are displayed together with TIME-GCM tides at the equator in Figure 1. As previously discussed, our analysis technique precludes the resolution of any migrating components. Thus, the zero amplitude DW1 and SW2 results illustrated in Figure 1 are nonphysical. Due to the slow precession of CHAMP through LT, as already discussed in the previous section, we have to keep in mind that the observed monthly tides are composites of 4 years, while TIME-GCM results represent 1 day in the indicated month. Also, in contrast to the simulated solar minimum conditions, the corresponding mean F10.7 value of the CHAMP data for the month of March is 128 sfu, for June 120 sfu, for September 122 sfu, and for December 118 sfu over the 4 years.

[12] Focusing first on the prominent DE3, it is clearly the dominant upper thermospheric nonmigrating tide in TIME-GCM. The biggest amplitude of 17.3 m/s is obtained in September. March and December reach amplitudes of 13.3 m/s and for June an amplitude of 7.2 m/s is calculated. The corresponding amplitude of DE3 for CHAMP is much smaller and displays different seasonal variability. DE3 amplitudes equal 3.9 m/s in March, 3.8 m/s in June, 7.7 m/s in September, and 2.5 m/s in December. *Häusler and Lühr* [2009] report that DE3 has a pronounced maximum between July and October peaking in July with an amplitude of 8.3 m/s and a smaller maximum in the month of April (4.4 m/s). Similar seasonal variation is reported for the observed temperature response in the lower thermosphere [*Forbes et al.*, 2008].

[13] The nonmigrating diurnal tide dominating the CHAMP tidal spectrum for the month of June is DE2 with an amplitude of 8.8 m/s. During December this tidal mode reaches an amplitude of 6.5 m/s, and in March and September, it reaches 3.8 m/s and 3.3 m/s, respectively.

Only in December can DE2 be found in the TIME-GCM tidal analysis with an amplitude of 9.2 m/s whereas for all the other months the DE2 amplitudes are below 1.6 m/s.

[14] Notably during March, September, and December, the SE2 dominates the TIME-GCM semidiurnal spectrum with amplitudes ranging from 4.4 m/s to 6.3 m/s. This behavior can be attributed to the strong DE3 and the nonlinear interaction between DE3 and DW1 resulting in the generation of SE2 and sPW4 [*Hagan et al.*, 2009]. In the CHAMP tidal analysis, SE2 is also present but with reduced amplitudes ranging from 1.4 m/s to 2.2 m/s. The model SE2 and the CHAMP SE2 exhibit very different behavior during the course of the year. Yet both TIME-GCM and CHAMP show similar amplitudes for sPW4 ranging from 1.0 m/s to 2.7 m/s for TIME-GCM and from 1.1 m/s to 3.0 m/s for CHAMP. The difference between the model and the satellite results is less than 0.7 m/s except for the month of June when the difference amounts to 2 m/s.

[15] Due to the fact that the June model run resulted in a reasonable DE3 amplitude, we decided to focus on June simulations for the investigation of a possible solar flux dependence. Therefore, we ran TIME-GCM for June setting the solar flux conditions to moderate (120 sfu) and high (200 sfu) levels but keeping all the other parameters described earlier constant. Figure 2 shows the results for the model simulations for different solar flux conditions. Displayed for comparison are the CHAMP results as presented in Figure 1. In general, one can say that the model predicts increasing amplitudes with increasing solar flux levels, though DE3 clearly decreases in amplitude with increasing solar flux level. Specifically, the DE3 amplitude decreased from 7.2 m/s for F10.7 = 75 sfu to 5.0 m/s for F10.7 = 120 sfu and to 2.1 m/s for F10.7 = 200 sfu.

[16] In order to investigate a possible solar flux dependence of the observed tides, we processed the CHAMP data differently. As already explained in the previous section, approximately 131 days of measurements are required to cover 24 h LT. Therefore, we utilized the described procedure to obtain the tidal signatures from 131 days of CHAMP data starting from day of year (DoY) 1 of 2002. We then moved the 131 days time window in steps of 11 days resulting in 122 individual running data sets for the available 4 years of measurements. The resultant June DE3, DE2, D0, and DW2 TIME-GCM and CHAMP signatures are displayed in Figure 3 for the three different solar flux levels. The corresponding time period for the CHAMP data is the 131 days time window centered around DoY 177 for 2002, DoY 175 for 2003, and DoY 170 for 2005. Within the aforementioned time windows, the solar flux level decreases from F10.7 = 175 sfu in 2002, to F10.7 = 128 sfu in 2003, and to F10.7 = 95 sfu in 2005. In addition to the solar flux dependence, Figure 3 also contains information about the latitudinal behavior of the reported tides. That is, the latitude range for TIME-GCM is 11.25°–31.25° and 31.25°–51.25° in the northern and southern hemispheres, respectively, in addition to the ±11.25° bin around the equator as previously discussed. The corresponding latitude bands for CHAMP are 10°–30° and 30°–50° in the northern and southern hemispheres, respectively, and ±10° around the equator.

[17] The latitudinal characteristics of DE3 illustrated in Figure 3 reveal striking similarities between the amplitudes of TIME-GCM and CHAMP, especially at the equator and in the southern hemisphere. Moreover, the CHAMP DE3 reveals the same solar flux dependence that is predicted by TIME-GCM. From 2002 to 2005, which corresponds to the declining phase of solar cycle 23, the amplitudes of DE3 observed by CHAMP are increasing from 3.2 m/s for F10.7 = 175 sfu to 7.0 m/s for F10.7 = 95 sfu at the equator where the DE3 maximum is also found. The DE2 observed by CHAMP is increasing with decreasing solar flux as well revealing an amplitude of 4.6 m/s for F10.7 = 175 sfu compared to 8.0 m/s for F10.7 = 95 sfu. The latitudinal structure of the CHAMP DE2 and DE3 is similar with larger amplitudes for DE2. As already mentioned, TIME-GCM does not resolve the DE2 very well. The amplitudes are mostly less than 2 m/s and therefore not significant enough to determine a solar flux dependence. The observed D0 tidal mode is prominent in the southern hemisphere, peaking at 40°S. Both TIME-GCM and CHAMP largely demonstrate this during low and middle solar activity. For high solar activity, CHAMP D0 amplitudes are much higher in the northern hemisphere and much lower at the equator and 20°S compared to TIME-GCM results. As already mentioned, the peak of these tidal modes are both found at 40°S, revealing an amplitude increase with increasing solar flux. The DW2 CHAMP and TIME-GCM comparison is inconclusive. Yet, the evolution of the CHAMP DW2 over the course of the 4 years (not shown) reveals an increase with increasing solar flux, which is also found in the TIME-GCM simulations (Figure 2).

4. Discussion and Summary

[18] We present, for the first time, a direct comparison of tidal signals in the zonal wind at upper thermospheric altitudes as observed in situ by CHAMP and obtained from TIME-GCM simulations. Special emphasis is put on the important DE3 nonmigrating tide which has strong effects on the neutral constituents of the upper atmosphere as demonstrated by *Oberheide et al.* [2009]. It is shown in Figure 1 that TIME-GCM is overestimating the strength of DE3 at 400 km altitude in all months except for June. Notably, we find the largest difference (10.8 m/s) between the model simulations and in situ measurements during December when CHAMP measures the smallest amplitudes of DE3. But, the intra-annual variation of DE3 in the zonal wind at upper thermospheric altitudes [*Häusler and Lühr*, 2009] is in good agreement with the reported annual characteristics of the zonal wind at 100 km altitude [e.g., *Pedatella et al.*, 2008] giving us confidence in the CHAMP results. Although TIME-GCM does not properly reproduce the observed DE3 intra-annual variability observed by CHAMP, the agreement between TIME-GCM and CHAMP for the month of June is remarkably good. The reported dependence of DE3 zonal wind amplitudes at 400 km altitude on solar flux level [*Oberheide et al.*, 2009] are also predicted by TIME-GCM. A decrease in solar flux level leads to an increase in DE3 amplitudes. *Oberheide et al.* [2009] attribute this effect to reduced tidal dissipation during solar minimum.

[19] Another diurnal tide exhibiting the same solar flux dependence as DE3 and which is quite prominent in the CHAMP data (actually exceeding DE3 in June) is DE2.

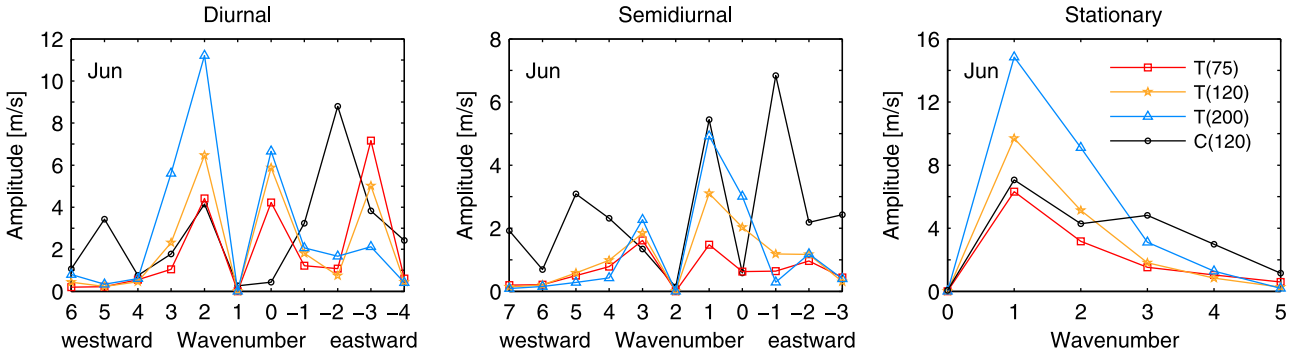

Figure 2. TIME-GCM June tidal spectra for three different solar flux levels: F10.7 = 75 sfu (square), F10.7 = 120 sfu (asterisk), F10.7 = 200 sfu (triangle) for (left) diurnal, (middle) semidiurnal, and (right) stationary components. Marked by circles are the tidal spectra from CHAMP with a solar flux average of F10.7 = 120 sfu for the months of June from 2002 to 2005. Positive (negative) wave numbers correspond to westward (eastward) propagating tides.

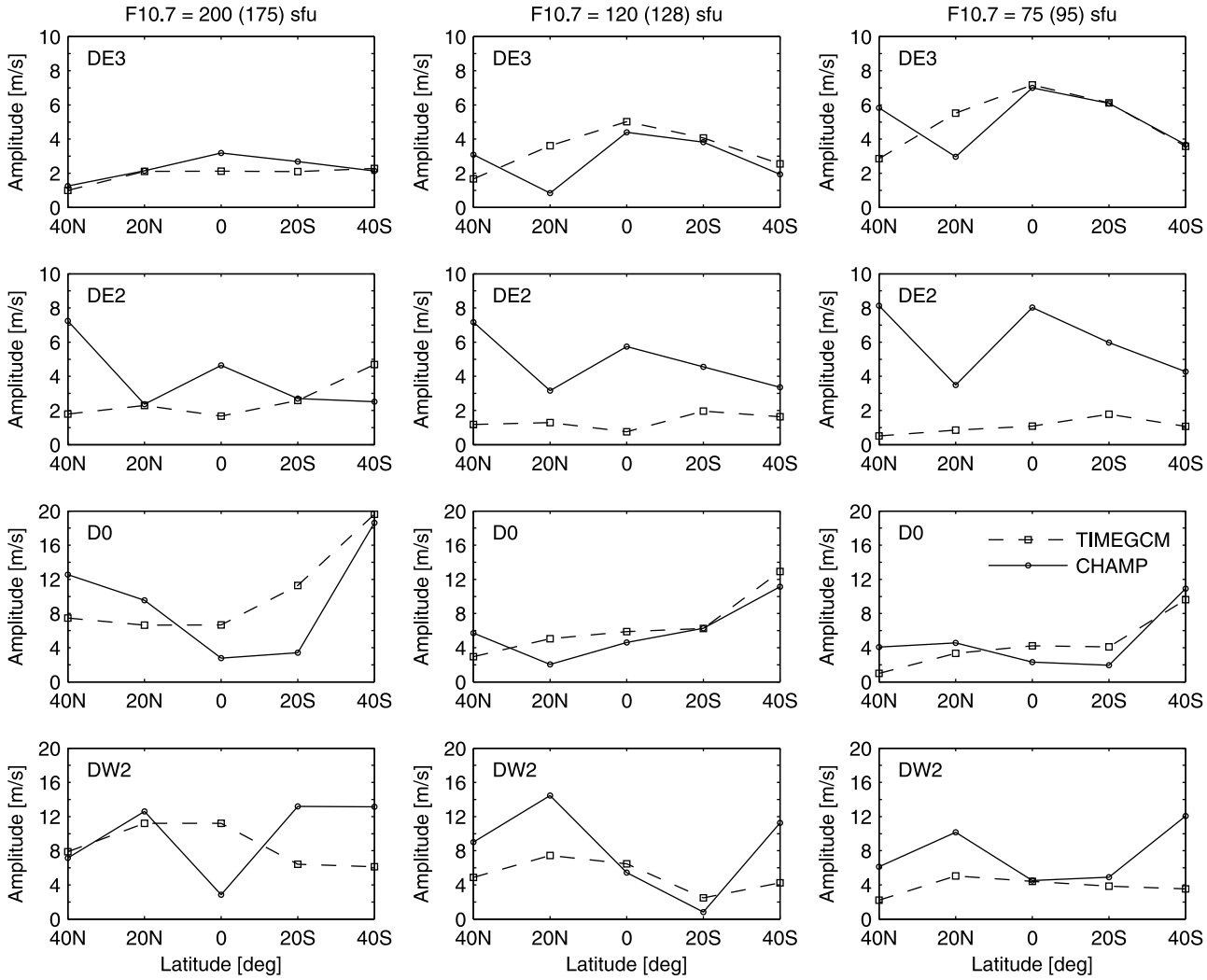

Figure 3. Latitudinal and solar cycle dependence of various tidal components in June. TIME-GCM (dashed line with squares) predictions and CHAMP (solid line with circles) observations of the components (top to bottom) DE3, DE2, D0, and DW2 for different flux levels: (left) F10.7 = 200 (175) sfu, (middle) F10.7 = 120 (128) sfu, and (right) F10.7 = 75 (95) sfu for TIME-GCM (CHAMP).

Again, the annual variation of DE2 observed by CHAMP [*Häusler and Lühr*, 2009] is in good agreement with other findings in the MLT region [e.g., *Pedatella et al.*, 2008], and recently *Forbes et al.* [2009] found also DE2 signatures in the temperature at 400 km altitude. Except for December, TIME-GCM underestimates DE2. But this is not surprising, since the GSWM DE2 amplitudes reported by *Hagan and Forbes* [2002] are also comparatively weak. The TIME-GCM DE2 discrepancies are actually attributable to a weakness in the GSWM lower boundary forcing. According to theory [*Hagan and Roble*, 2001], the nonlinear interaction between DE2 and DW1 yields the generation of SE1 and sPW3, similar to the SE2 and sPW4 resulting from DE3 and DW1 interaction as reported by *Hagan et al.* [2009]. In fact, we observe with CHAMP a strong SE1 with an amplitude of 6.8 m/s and sPW3 is displaying an amplitude of 4.8 m/s when DE2 reaches its maximum in June (Figure 1). Due to the fact that TIME-GCM does not correctly represent the measured DE2 amplitudes at present, a connection between DE2, SE1 and sPW3 cannot yet be confirmed. Notably, we observe the same solar dependence for CHAMP SE1 and sPW3, as well as SE2 and sPW4, that we observe for DE2 and DE3 (not shown).

[20] Except for December, the agreement between TIME-GCM and CHAMP for the diurnal westward propagating tides is rather good although the model does not predict DW5. An increase of DW2 amplitudes with increasing solar flux can be confirmed by CHAMP observations although it is not so evident from Figure 3. Further, we see that DW2 does not peak at the equator but has rather larger amplitudes at midlatitudes.

[21] TIME-GCM predicts an increase of the standing diurnal tide during solar maximum conditions at the equator for June (Figure 2). The amplitude increase cannot be confirmed by CHAMP data, but CHAMP does not observe large amplitudes of D0 at the equator during June after all. Yet, when looking at midlatitudes (Figure 3), an excellent agreement is found between TIME-GCM and CHAMP for 40°S. D0 is more pronounced in the southern hemisphere with larger amplitudes for higher solar flux levels.

[22] CHAMP observes a strong SW1 in June and December and a strong SW3 in September (Figure 1) which is not predicted by TIME-GCM at all. At present, we cannot offer an explanation for the discrepancy.

[23] In summary, the comparison between TIME-GCM and CHAMP demonstrates that the model is capable of reproducing the observed dependence on solar flux of the tides that remain significant in the model at 400 km altitude, i.e., DE3, DW2, and D0. Specifically, DW2 and D0 amplitudes increase with increasing solar flux, while DE3 amplitudes decrease during solar maximum conditions. Nevertheless, TIME-GCM exhibits a weakness in simulating the observed intra-annual variation of the various tides. This is at least partly due to insufficient lower boundary forcing, but we also cannot rule out inaccuracies in the model dissipation schemes. However, we are confident that we can overcome the discrepancies between TIME-GCM and the observations, and we will use the model to explore the open issues of dynamical coupling between the various atmospheric layers. As a first step, we plan to update the TIME-GCM lower boundary conditions with new GSWM forcing that is currently in development.

[24] **Acknowledgments.** K.H. is supported by the DFG through its Priority Program CAWSES (SPP1176), grant LU446/9-1, and by the Graduate Student Visitor Program of the Advanced Study Program of the National Center for Atmospheric Research. The National Center for Atmospheric Research is sponsored by the National Science Foundation.

References

Chapman, S., and R. S. Lindzen (1970), *Atmospheric Tides: Thermal and Gravitational*, D. Reidel, Dordrecht, Netherlands.

England, S. L., S. Maus, T. J. Immel, and S. B. Mende (2006), Longitude variation of the E-region electric fields caused by atmospheric tides, *Geophys. Res. Lett.*, *33*, L21105, doi:10.1029/2006GL027465.

Evans, D. S. (1987), Global statistical patterns of auroral phenomena, in *Proceedings of the Symposium on Quantitative Modeling of Magneto-spheric-Ionospheric Coupling Processes*, edited by Y. Kamide and R. A. Wolf, pp. 325–330, Kyoto Sangyo Univ., Kyoto, Japan.

Forbes, J. M. (1995), Tidal and planetery waves, in *The Upper Mesosphere and Lower Thermosphere: A Review of Experiment and Theory*, *Geophys. Monogr. Ser.*, vol. 87, edited by R. M. Johnson and T. L. Killeen, pp. 49–65, AGU, Washington, D. C.

Forbes, J. M., J. Russell, S. Miyahara, X. Zhang, S. Palo, M. Mlynczak, C. J. Mertens, and M. E. Hagan (2006), Troposphere-thermosphere tidal coupling as measured by the SABER instrument on TIMED during July–September 2002, *J. Geophys. Res.*, *111*, A10S06, doi:10.1029/2005JA011492.

Forbes, J. M., X. Zhang, S. Palo, J. Russell, C. J. Mertens, and M. Mlynczak (2008), Tidal variability in the ionospheric dynamo region, *J. Geophys. Res.*, *113*, A02310, doi:10.1029/2007JA012737.

Forbes, J. M., S. L. Bruinsma, X. Zhang, and J. Oberheide (2009), Surface-exosphere coupling due to thermal tides, *Geophys. Res. Lett.*, *36*, L15812, doi:10.1029/2009GL038748.

Hagan, M. E., and J. M. Forbes (2002), Migrating and nonmigrating diurnal tides in the middle and upper atmosphere excited by tropospheric latent heat release, *J. Geophys. Res.*, *107*(D24), 4754, doi:10.1029/2001JD001236.

Hagan, M. E., and J. M. Forbes (2003), Migrating and nonmigrating semidiurnal tides in the upper atmosphere excited by tropospheric latent heat release, *J. Geophys. Res.*, *108*(A2), 1062, doi:10.1029/2002JA009466.

Hagan, M. E., and R. G. Roble (2001), Modeling the diurnal tidal variability with the National Center for Atmospheric Research thermosphere-ionosphere-mesosphere-electrodynamics general circulation model, *J. Geophys. Res.*, *106*(A11), 24,869–24,882.

Hagan, M. E., A. Maute, R. G. Roble, A. D. Richmond, T. J. Immel, and S. L. England (2007), Connections between deep tropical clouds and the Earth's ionosphere, *Geophys. Res. Lett.*, *34*, L20109, doi:10.1029/2007GL030142.

Hagan, M. E., A. Maute, and R. G. Roble (2009), Tropospheric tidal effects on the middle and upper atmosphere, *J. Geophys. Res.*, *114*, A01302, doi:10.1029/2008JA013637.

Hartman, W. A., and R. A. Heelis (2007), Longitudinal variations in the equatorial vertical drift in the topside ionosphere, *J. Geophys. Res.*, *112*, A03305, doi:10.1029/2006JA011773.

Häusler, K., and H. Lühr (2009), Nonmigrating tidal signals in the upper thermospheric zonal wind at equatorial latitudes as observed by CHAMP, *Ann. Geophys.*, *27*, 2643–2652.

Häusler, K., H. Lühr, S. Rentz, and W. Köhler (2007), A statistical analysis of longitudinal dependences of upper thermospheric zonal winds at dip equator latitudes derived from CHAMP, *J. Atmos. Sol. Terr. Phys.*, *69*, 1419–1430, doi:10.1016/j.jastp.2007.04.004.

Immel, T. J., E. Sagawa, S. L. England, S. B. Henderson, M. E. Hagan, S. B. Mende, H. U. Frey, C. M. Swenson, and L. J. Paxton (2006), Control of equatorial ionospheric morphology by atmospheric tides, *Geophys. Res. Lett.*, *33*, L15108, doi:10.1029/2006GL026161.

Kil, H., S.-J. Oh, M. C. Kelley, L. J. Paxton, S. L. England, E. R. Talaat, K.-W. Min, and S.-Y. Su (2007), Longitudinal structure of the vertical $\times$ drift and ion density seen from ROCSAT-1, *Geophys. Res. Lett.*, *34*, L14110, doi:10.1029/2007GL030018.

Lin, C. H., W. Wang, M. E. Hagan, C. C. Hsiao, T. J. Immel, M. L. Hsu, J. Y. Liu, L. J. Paxton, T. W. Fang, and C. H. Liu (2007), Plausible effect of atmospheric tides on the equatorial ionosphere observed by the FORMOSAT-3/COSMIC: Three-dimensional electron density structures, *Geophys. Res. Lett.*, *34*, L11112, doi:10.1029/2007GL029265.

Lühr, H., K. Häusler, and C. Stolle (2007), Longitudinal variation of *F* region electron density and thermospheric zonal wind caused by atmospheric tides, *Geophys. Res. Lett.*, *34*, L16102, doi:10.1029/2007GL030639.

Lühr, H., M. Rother, K. Häusler, P. Alken, and S. Maus (2008), The influence of nonmigrating tides on the longitudinal variation of the equatorial electrojet, *J. Geophys. Res.*, *113*, A08313, doi:10.1029/2008JA013064.

Oberheide, J., Q. Wu, T. L. Killeen, M. E. Hagan, and R. G. Roble (2006), Diurnal nonmigrating tides from TIMED Doppler Interferometer wind data: Monthly climatologies and seasonal variations, *J. Geophys. Res.*, *111*, A10S03, doi:10.1029/2005JA011491.

Oberheide, J., J. M. Forbes, K. Häusler, Wu, and S. L. Bruinsma (2009), Tropospheric tides from 80 to 400 km: Propagation, interannual variability, and solar cycle effects, *J. Geophys. Res.*, *114*, D00I05, doi:10.1029/2009JD012388.

Pedatella, N. M., J. M. Forbes, and J. Oberheide (2008), Intra-annual variability of the low-latitude ionosphere due to nonmigrating tides, *Geophys. Res. Lett.*, *35*, L18104, doi:10.1029/2008GL035332.

Roble, R. G. (1995), Energetics of the mesosphere and thermosphere, in *The Upper Mesosphere and Lower Thermosphere: A Review of Experiment and Theory*, *Geophys. Monogr. Ser.*, vol. 87, edited by R. M. Johnson and T. L. Killeen, pp. 1–21, AGU, Washington, D. C.

Roble, R. G. (1996), The NCAR thermosphere-ionosphere-mesosphere-electrodynamics general circulation model (TIME-GCM), in *STEP Handbook on Ionospheric Models*, edited by R. W. Schunk, pp. 281–288, Utah Sate Univ., Logan.

Roble, R. G., and E. C. Ridley (1994), A thermosphere-ionosphere-mesosphere-electrodynamics general circulation model (time-GCM): Equinox solar cycle minimum simulations (30–500 km), *Geophys. Res. Lett.*, *21*, 417–420, doi:10.1029/93GL03391.

Sagawa, E., T. J. Immel, H. U. Frey, and S. B. Mende (2005), Longitudinal structure of the equatorial anomaly observed by IMAGE/FUV, *J. Geophys. Res.*, *110*, A11302, doi:10.1029/2004JA010848.

Talaat, E. R., and R. S. Lieberman (1999), Nonmigrating diurnal tides in mesospheric and lower-thermospheric winds and temperatures, *J. Atmos. Sci.*, *56*(24), 4073–4087.

Wu, Q., D. A. Ortland, T. L. Killeen, R. G. Roble, M. E. Hagan, H.-L. Liu, S. C. Solomon, J. Xu, W. R. Skinner, and R. J. Niciejewski (2008), Global distribution and interannual variations of mesospheric and lower thermospheric neutral wind diurnal tide: 2. Nonmigrating tide, *J. Geophys. Res.*, *113*, A05309, doi:10.1029/2007JA012543.

Zhang, X., J. M. Forbes, M. E. Hagan, J. M. Russell III, S. E. Palo, C. J. Mertens, and M. G. Mlynczak (2006), Monthly tidal temperatures 20–120 km from TIMED/SABER, *J. Geophys. Res.*, *111*, A10S08, doi:10.1029/2005JA011504.

M. E. Hagan, A. Maute, and R. G. Roble, High Altitude Observatory, National Center for Atmospheric Research, Boulder, CO 80307, USA.

K. Häusler and H. Lühr, Helmholtz Centre Potsdam–GFZ German Research Centre for Geosciences, Telegrafenberg, D-14473 Potsdam, Germany. (kathrin@gfz-potsdam.de)